A Spectrum Synch Technique for Induction Motor Health Condition Monitoring

De Z. Li, Wilson Wang, *Senior Member, IEEE*, and Fathy Ismail

***Abstract*—Induction motors (IMs) are commonly used in various industrial applications. A spectrum synch (SS) technique is proposed in this paper for early IM defect detection using electric current signals; fault detection in this paper will focus on defects in rolling element bearings and rotor bars, which together account for more than half of IM imperfections. In bearing fault detection, the proposed SS technique will highlight the peakedness of the fault frequency components distributed over several fault-related local bands. These bands are synchronized to form a fault information spectrum to accentuate fault features. A central kurtosis indicator is proposed to extract representative features from the fault information spectrum and formulates a fault index for incipient IM fault diagnosis. The effectiveness of the developed SS technique is demonstrated on IM with broken rotor bars and IM with damaged bearing. Test results show that the developed SS technique can detect incipient IM faults effectively.**

***Index Terms*—Bearing fault detection, broken rotor bars, current signal, induction motor (IM), spectrum synch (SS) analysis.**

I. Introduction

INDUCTION motors (IMs) are the workhorse of many industries. IM fault detection and online monitoring have become important aspects to improve productivity and reduce maintenance cost. The IM faults can be classified into two categories: mechanical faults and electrical defects. Mechanical faults include: bearing defects, air gap eccentricity, shaft misalignment; electrical faults encompass stator winding defect, broken rotor bars, etc. [1]. Investigations have revealed that faults in rolling element bearings account for about 75% of small and medium motor defects and 41% of large motor defects, whereas broken rotor bar faults account for 10% of the motor imperfections in domestic and industrial applications [2]. Accordingly, this paper will focus on IM defect detection associated with rolling element bearings and broken rotor bars.

IM fault detection can be performed based on the analysis of vibration signals and/or stator current signals. Although the former has higher signal-to-noise ratio (SNR), the vibration sensors are more expensive and sensitive to installation location [3]–[5]. Accordingly, current signals will be used in this paper for IM health condition monitoring.

The bearing fault detection using the current signal could be a challenging task since the related signals are usually weak and modulated by other strong signatures. Moreover, the complex signal transmission route from bearing vibration to stator current poses higher impedance and hence results in lower SNR [6], [7]. Several works have been undertaken on IM bearing fault detection [8]–[10]. Schoen *et al.* presented a bearing fault model in [11] to recognize IM bearing fault information. This bearing fault model was then improved by Blödt *et al.* [12] to enhance bearing fault characteristic frequencies. Ilonen *et al.* used statistical discriminative measures to extract features of different IM conditions, in order to improve bearing fault detection accuracy [13]. Eren *et al.* applied wavelet packet decomposition to analyze nonstationary current signals [14], whereas Zhou *et al.* employed Wiener filter to remove nonbearing fault frequency components [15]. The aforementioned techniques, however, only examine the information about a few specific characteristic frequencies rather than spectral features over their neighborhood bands. These approaches may result in less reliable IM condition monitoring in terms of false alarms and missed alarms.

Rotor bar breakage is another common IM defect. A rotor bar could be damaged partially or completely due to excessive thermal stress, or manufacturing defects, or of both. Many researchers have been working on IM broken rotor bar fault detection. For example, Kim *et al*. presented a technique to detect broken rotor bar fault in inverter-fed IMs under the standstill condition [16]. Ordaz-Moreno *et al.* suggested a simplified algorithm to detect broken rotor bar fault online [17]. Ayhan *et al.* employed the Fourier transform (FT) and autoregressive-based spectrum method for IM broken rotor bar fault diagnosis with low sampling frequency [18]. Haji *et al.* utilized a Bayes minimum error classifier to detect IM broken rotor bar defect under steady state condition [19]. Zhang *et al.* employed the wavelet ridge to detect broken rotor bars from IM starting current [20]. Kim *et al.* suggested a high-resolution parameter estimation method to diagnose motor rotor bar breakage [21]. Soualhi *et al.* employed the artificial ant clustering method to facilitate motor fault detection [22]. Rangel-Magdaleno *et al.* used mathematical morphology and motor current signature analysis for broken bars detection [23]. Xu *et al.* utilized estimation of signal parameters via the rotational invariance technique and the Hilbert method to detect rotor fault at low slip [24]. Most of the aforementioned techniques examine some specific features in the spectrum to detect the IM fault. Some high amplitude outliers in the neighborhood local bands may interfere in the

Manuscript received July 4, 2014; revised January 10, 2015; accepted May 18, 2015. Date of publication July 29, 2015; date of current version November 20, 2015. This work was supported in part by the Natural Sciences and Engineering Research Council of Canada and in part by eMech Systems, Inc. Paper no. TEC-00480-2014.

D. Z. Li and F. Ismail are with the Department of Mechanical and Mechatronics Engineering, University of Waterloo, Waterloo, ON N2L 3G1, Canada (e-mail: d45li@uwaterloo.ca; fmismail@uwaterloo.ca).

W. Wang is with the Department of Mechanical Engineering, Lakehead University, Thunder Bay, ON P7B 5E1, Canada (e-mail: Wilson.Wang@Lakeheadu.ca).

Color versions of one or more of the figures in this paper are available online at http://ieeexplore.ieee.org.

Digital Object Identifier 10.1109/TEC.2015.2454440

detection of these fault-related features, and therefore lower the reliability of the fault detection.

To tackle the aforementioned difficulties, a spectrum synch (SS) technique is proposed in this paper for incipient IM fault detection. The SS will examine characteristic frequency components as well as their features over their neighborhood local bands, in order to comprehensively highlight fault features, and mitigate the effects of high amplitude outliers. The proposed SS technique is new in the following aspects.

1) A synch technique is proposed to form fault information spectrum (FIS) by synchronizing several fault-related local bands, so as to accentuate the fault features.
2) A central kurtosis technique is suggested to extract fault information from the resulting FIS, and generate a fault indicator for incipient IM fault detection. The effectiveness of the proposed SS technique is verified by IM broken rotor bar fault detection and IM bearing fault detection.

The remainder of this paper is organized as follows: the developed SS technique is described in Section II; in Section III, the effectiveness of the proposed diagnostic tool is examined by using two common types of IM fault conditions; finally, some concluding remarks of this study are summarized in Section IV.

II. SS Technique for IM Health Condition Monitoring

The proposed SS technique is composed of two procedures: local band synch and central kurtosis analysis. The local band synch is used to form the FIS and enhance fault features. The central kurtosis indicator is suggested to generate a fault index for IM health condition monitoring. Details will be discussed in this section.

A. Local Band Synch

The IM fault characteristic frequency components are distributed over the spectrum, which are, however, usually difficult to recognize due to their low amplitude. To highlight the fault features in the spectrum, the proposed FIS aims to enhance the local peakedness of the fault frequency components. First, to lessen the noise effect in the IM current signal, the spectrum averaging of *J* datasets ϕ_j; $j = 1, 2, \ldots, J$, is taken to improve the SNR, computed by

$$\Phi = \frac{1}{J}\sum\nolimits_{j=1}^{J} \log\left(P(\phi_j)\right) \tag{1}$$

where Φ is the spectrum average; $P(\phi_j)$ represents the nonparametric power spectral density (PSD) estimate of the dataset [25], given by

$$P(\phi_j) = \frac{2}{f_s N}\sum_{i=1}^{N/2+1} |F_j(i))|^2 \tag{2}$$

where F_j is the spectrum of ϕ_j using the FT; *N* is the length of ϕ_j; and f_s is the sampling frequency.

The fault features are related to fault characteristic frequencies, most of which over the local bands are masked by some other higher level signals considered as noise. To tackle this problem, the local bands containing the fault characteristic frequencies are synchronized to reduce the noise effect and protrude the fault frequency components. In each selected local band, the theoretically calculated fault frequency component f_c is located in the center of the window, and the width of the local band is selected to properly reveal the peakedness of f_c.

To synchronize the corresponding bands at different locations (frequencies) of the spectrum, the spectrum is transformed from frequency domain $\Phi(f)$ to discrete point representation $\Phi(d)$. Each frequency *f* can be represented by its nearest discrete point *d*. Then, fault characteristic frequency $f_c(k)$ is transformed into a discrete point, $d_c(k)$, whose corresponding frequency is the one closest to f_c, where $k = 1, 2, \ldots, K$, and *K* is the total number of fault characteristic frequencies considered. Thus, *K* local bands will be used for this synch operation. The widths of local bands are set identical in this work to facilitate the synch operation. Given the bandwidth in frequency b_w, the length of the local band in discrete point representation, d_w, will be

$$d_w = 2R\left\langle \frac{1}{2} b_w \frac{D_s}{f_s} \right\rangle \tag{3}$$

where f_s is the sampling frequency in Hz, D_s is the discrete point representing f_s, and $R\langle\bullet\rangle$ represents round-off operation. The *k*th local band ψ_k in the discrete point representation can be determined by

$$\psi_k = \{\Phi(i)\}_{i=d_c(k)-\frac{1}{2}d_w,\ldots,d_c(k)+\frac{1}{2}d_w} - \frac{1}{d_w+1}\sum\nolimits_{i=d_c(k)-\frac{1}{2}d_w}^{d_c(k)+\frac{1}{2}d_w} \Phi(i). \tag{4}$$

The *i*th discrete point in the *k*th local band ψ_k is denoted as $\psi_{i,k}$; $i = 1, 2, \ldots, d_w + 1$; $k = 1, 2, \ldots, K$. The *i*th discrete points over *K* local bands $\{\psi_{i,k}\}$ are sorted in a descending order in term of their values to generate $\pi_{i,k}$, $k = 1, 2, \ldots, K$. The central point of FIS (i.e., $i = \frac{1}{2}d_w + 1$) is formulated as

$$g_i = \begin{cases} \frac{2}{K}\sum\limits_{j=1}^{K/2} \pi_{i,j} & \text{if } K \text{ is even} \\ \frac{2}{(K+1)}\sum\limits_{j=1}^{(K+1)/2} \pi_{i,j} & \text{if } K \text{ is odd} \end{cases}, i = \frac{1}{2}d_w + 1. \tag{5}$$

Other points of FIS are formulated as

$$g_i = \xi\left\{\pi_{i,j}\right\}_{j=1,2,\ldots,K}, i = 1, 2, \ldots, \frac{1}{2}d_w, \frac{1}{2}d_w + 2, \ldots, d_w + 1 \tag{6}$$

where $\xi\{\bullet\}$ represents the computation of median value. The top 50% high amplitude fault characteristic frequency components or center frequency components in local bands are averaged in (5) to enhance the fault features. The median value calculation in (6) will suppress other frequency components in the local bands and reduce the amplitude of outliers. The processing procedures of the proposed FIS formation are illustrated in Fig. 1, where the frequency resolution $\Delta f = 0.5$ Hz.

B. Central Kurtosis Indicator

The classic kurtosis is a measure of the peakedness of a signal, computed as $\chi = \mu_4/\sigma^4$, where σ and μ_4 are the standard deviation and the fourth moment of the signal distribution, respectively. The classic kurtosis measures all peaked frequency

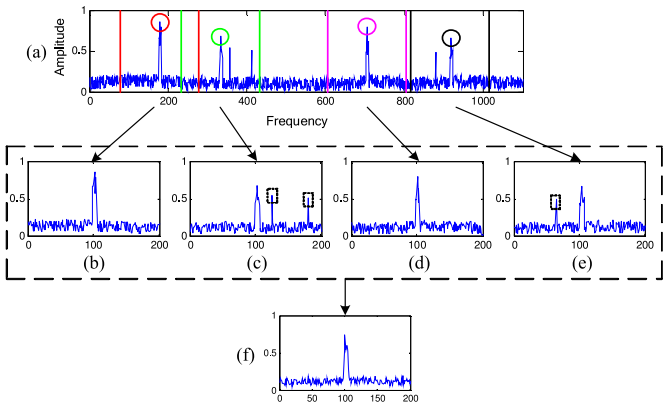

Fig. 1. Formulation of FIS. (a) Original spectrum. (b)–(e) Respective extracted local bands corresponding to the four circled fault frequency components (red, green, pink, and black). (f) Formulated FIS. The dotted lines in graph (a) represent the boundaries of the local bands; the dashed rectangular represent outliers in the local bands.

components of the FIS, which may not properly reveal the fault information. In this paper, the fault detection aims to evaluate the peakedness of the center frequency component in the FIS. Therefore, a central kurtosis indicator is proposed in this paper to facilitate fault detection. Given the FIS $g(i)$; $i = 1, 2, \ldots, d_w + 1$, the relative amplitude of the center frequency components can be determined by

$$\nu_s = g_s - \xi\{g\} \tag{7}$$

where $g_s = \{g_i\}_{i=d_w/2+1}$ is the center discrete point in the FIS. The amplitude of fault frequency component over synchronized local bands (i.e., FIS), rather than the entire spectrum as in the classical methods, is used to examine fault information.

The variation of the FIS excluding center frequency component g_s can be evaluated by

$$\sigma_s = E\left\{\left(\tilde{g} - \xi\{\tilde{g}\}\right)^2\right\}^{\frac{1}{2}} \tag{8}$$

where $E\{\bullet\}$ represents the expectation function, and $\tilde{g} = \{g_i, i = 1, 2, \ldots, d_w/2, d_w/2 + 2, \ldots, d_w + 1\}$.

Then, the peakedness of the fault frequency component in the FIS can be measured by the central kurtosis, determined by

$$\chi_s = \begin{cases} \nu_s^4/\sigma_s^4 & \text{if} \quad \nu_s > 0 \\ 0 & \text{if} \quad \nu_s \leq 0. \end{cases} \tag{9}$$

C. Implementation of the SS Technique

To recapitulate, the proposed SS technique is implemented for IM defect detection with the following steps.

1) Collect J electric current datasets $\phi_j, j = 1, 2, \ldots, J$, with the same time delay.
2) Determine the spectrum average Φ. Then, extract characteristic local bands using (4), and synchronize the local bands to form the FIS using (5) and (6), to reduce the noise effect and highlight the fault features.
3) Compute the center frequency representative feature using (7), and the variation of the FIS using (8). The fault diagnosis can be performed by analyzing the central kurtosis computed from (9).

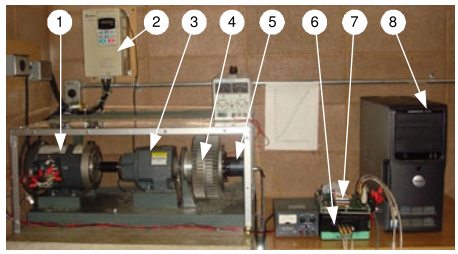

Fig. 2. IM experimental setup: (1) tested IM, (2) speed controller, (3) gearbox, (4) load system, (5) encoder, (6) current sensors, (7) data acquisition system, (8) computer.

III. IM Fault Detection Applications

To evaluate the effectiveness of the proposed SS technique for IM fault detection, a series of tests have been conducted for the two common types of IM defects, IM broken rotor bar fault and IM bearing defect, using stator current signals. In rolling element bearings, defect occurs on the race of the fixed ring first since fixed ring material over the load zone undertakes more cycles of fatigue loading than other bearing components (e.g., the rotating ring and rolling elements). Correspondingly, this test focuses on incipient bearing defect, or fault on the outer race (fixed ring in this case).

A. Experimental Setup

Fig. 2 shows the experimental setup used in this test. The tested IMs (3-phase, 2-pole, 50 Hz, 1/3 hp) are made by Marathon Electric, each having 34 rotor bars and 24 stator slots. Its speed is controlled by a speed controller (VFD-B from Delta Electronics) with output frequency 0.1–400 Hz. A magnetic clutch system (PHC-50 from Placid Industries) is used as the dynamometer to provide external loading, with torque ranging from 1 to 40 N·m. A gearbox (Boston Gear 800) is used to adjust the speed ratio of the dynamometer. An encoder (NSN-1024-2M-F) is used to measure the shaft speed. Stator current signals are measured by the use of current sensors (LTS 6-NP). A data acquisition board (Quanser Q4) is used for signal measurement.

B. Broken Rotor Bar Fault Detection

The fault detection of IM broken rotor bar defect is generally based on spectral analysis by inspecting sideband components of fault indicator in the spectrum

$$f_{bl} = (1 - 2ks)\, f_p \tag{10}$$

$$f_{br} = (1 + 2ks)\, f_p \tag{11}$$

where f_{bl} and f_{br} are the respective left sideband and right sideband of the IM broken rotor bar fault, $k = 1, 2, \ldots$; f_p is the power supply frequency of the IM; $s = \frac{n_s - n_a}{n_s} \times 100\,\%$ is the slip of the IM. n_s (r/min) is the speed of rotating magnetic field, and n_a (r/min) is the shaft rotating speed. In the following tests, IMs with one broken rotor bar, two broken rotor bars, and

three broken rotor bars are used to evaluate the proposed SS technique.

To evaluate the proposed SS technique, the PSD-based fault detection is used for comparison. In the PSD-based fault detection, the fault indicator can be represented as

$$\chi_p = \begin{cases} \nu_p^4/\sigma_p^4 & \text{if} \quad \nu_p > 0 \\ 0 & \text{if} \quad \nu_p \leq 0 \end{cases} \tag{12}$$

where ν_p represents the averaged amplitude of fault frequency components, σ_p represents the standard deviation of the averaged local band, and χ_p is the fault indicator. A discrete wavelet transform (DWT)-based fault detection method [26] is also used for comparison, which can be represented by

$$\chi_d = F_c/E_c \tag{13}$$

where E_c is mean current; F_c is the root mean square value of detail level in DWT containing fault frequency components of interests.

1) Full-Load Condition: First test aims to detect the IM broken rotor bar fault, 50 Hz power supply frequency, and full-load condition ((100% of rated power)). To reduce the noise effect in the spectrum, 20 datasets are collected for spectrum averaging (i.e., $J = 20$). Other settings are $f_s = 16\,384$ Hz and $b_w = 6$ Hz. The frequency band [32 Hz 68 Hz] is used to detect broken rotor fault, because the amplitudes of high-order [i.e., k in (10) and (11)] characteristic frequencies are not prominent in the spectrum. Fig. 3 illustrates the PSD of a healthy IM [see Fig. 3(a)], and PSDs of IMs with one broken rotor bar [see Fig. 3(b)], two broken rotor bars [see Fig. 3(c)], and three broken rotor bars [see Fig. 3(d)]. From Fig. 3(b)–(d), it is seen that the magnitude of broken rotor bar fault frequency components varies and some are not prominently protruded. Therefore, a better fault detection technique is needed to extract useful information from multiple characteristic frequency components in the spectrum to generate a more reliable fault indicator.

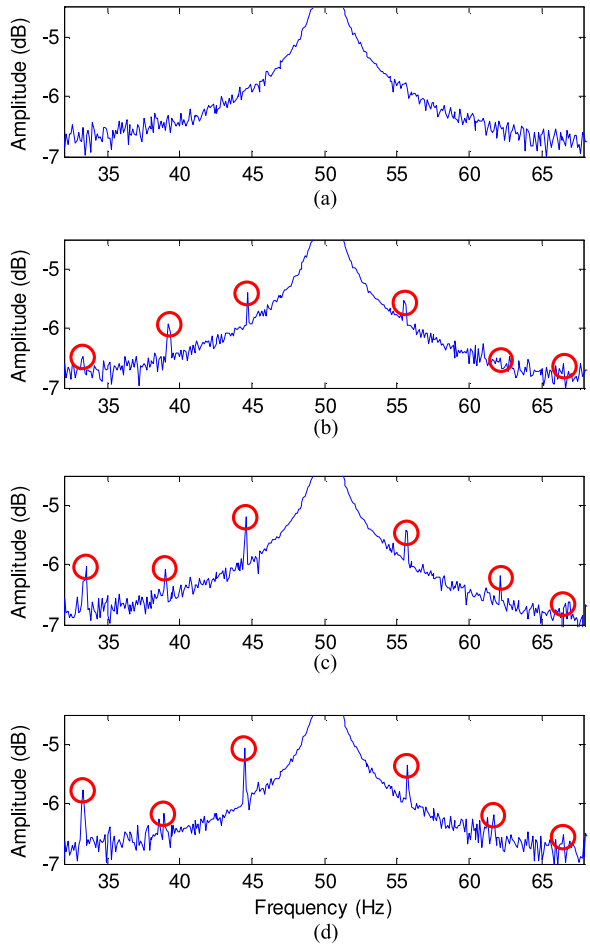

Fig. 3. Spectrum average Φ corresponding to (a) healthy IM, (b) IM with one broken rotor bar, (c) IM with two broken rotor bars, and (d) IM with three broken rotor bars, under full-load condition. The red solid circles specify fault frequency components.

The FIS, corresponding to a healthy IM [see Fig. 3(a)], one broken rotor bar-faulted IM [see Fig. 3(b)], two broken rotor bars-faulted IM [see Fig. 3(c)], and three broken rotor bar-faulted IM [see Fig. 3(d)] are given in Fig. 4(a), (b), (c), and (d), respectively. It is seen from Fig. 4 that the center frequency components (i.e., synchronized broken rotor bar fault frequency components) in Fig. 4(b)–(d) have higher relative amplitude than that in Fig. 4(a), which is evaluated by the indicator ν_s in the proposed SS technique. The spectrum variations of Fig. 4(b)–(d) are similar to that of Fig. 4(a), which is examined by the value σ_s in the SS technique. Therefore, the fault information in the FIS can be characterized by the indicator χ_s using the proposed SS technique.

The mean value of E_c and F_c (i.e., root mean square value of detail level 9 (D9) in DWT) over 20 runs is shown in Table I. D9 corresponds to frequency band [32 Hz 64 Hz], which contains main broken rotor bar fault frequency components. The mean value of indicators corresponding to PSD and the proposed SS and running time over 20 runs are also summarized in Table I. ν represents ν_p in the PSD method or ν_s in the SS method; σ represents σ_p in the PSD method or σ_s in the SS method. χ represents χ_p in PSD or χ_s in SS or χ_d in DWT. The values of slip for IMs with healthy condition, one broken bar, two broken bars, and three broken bars are 0.048, 0.049, 0.050, and 0.049, respectively. From Table I, it is seen that it is difficult to differentiate the IM broken rotor bar fault condition from the IM healthy condition using DWT, because the interested detail level contains high amplitude interference such as supply frequency component. The PSD and SS can be used to detect broken rotor bar fault because the value χ of faulted IM is larger than that of the healthy IM. Moreover, the value of χ increases as the number of broken bars increases by using SS. Consequently, the proposed SS technique can be used as an effective indicator for IM broken rotor bar fault detection under full-load condition.

2) Half-Load Condition: The proposed SS technique is then used for IM broken rotor bar fault detection with 50 Hz supply frequency and half-load condition (50% of rated power). Other settings remain the same as in previous tests. The spectrum of frequency band [32 Hz 68 Hz] is used for fault diagnosis. Fig. 5 shows the PSD of a healthy IM [see Fig. 5(a)], and PSDs of IMs with one broken rotor bar [see Fig. 5(b)], two broken rotor bars [see Fig. 5(c)], and three broken rotor bars [see Fig. 5(d)]. The corresponding FIS is given in Fig. 6. The related

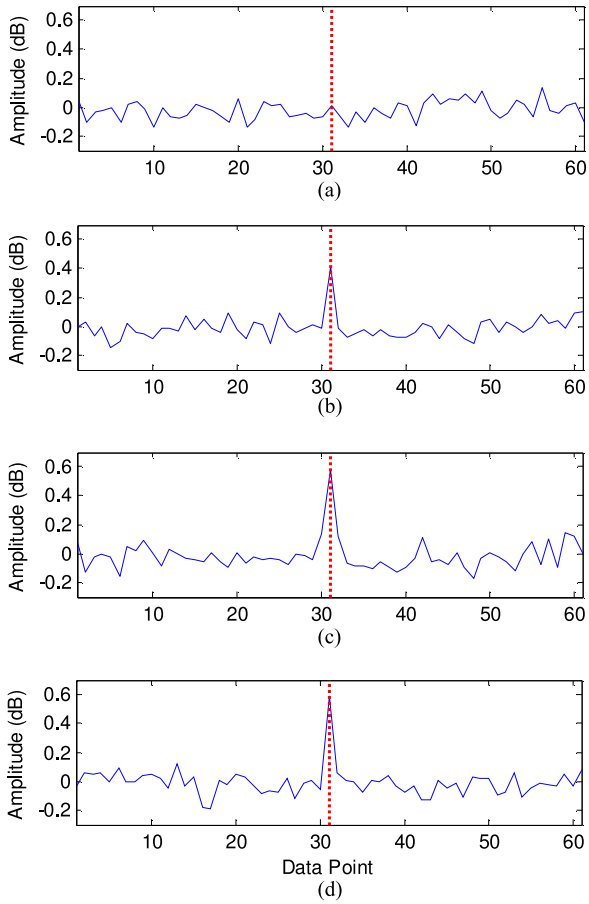

Fig. 4. FIS generated by the SS technique under full-load condition from: (a) healthy IM; (b) IM with one broken rotor bar; (c) IM with two broken rotor bars; and (d) IM with three broken rotor bars.

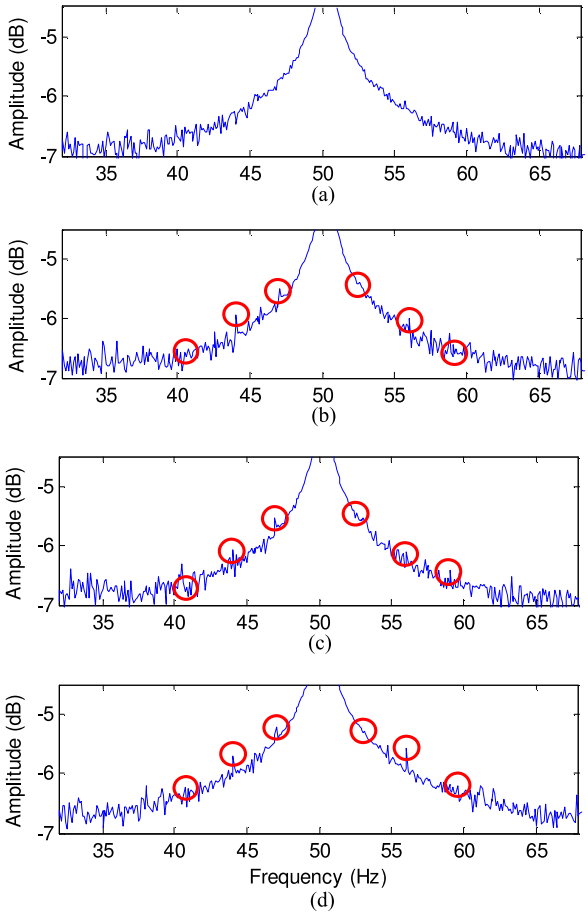

Fig. 5. Spectrum average Φ corresponding to (a) healthy IM, (b) IM with one broken rotor bar, (c) IM with two broken rotor bars, and (d) IM with three broken rotor bars, under half-load condition. The red solid circles highlight fault frequency components.

TABLE I
COMPARISONS OF MEAN VALUES OF INDICATORS FOR IM BROKEN ROTOR BAR FAULT DETECTION OVER 20 RUNS UNDER FULL-LOAD CONDITION

Indicators		$F_c(A)$	$E_c(A)$	v (dB)	σ (dB)	χ	Time (s)
PSD	Healthy	—	—	0.231	0.190	2.185	0.588
	1 Br	—	—	0.339	0.205	7.478	0.608
	2 Brs	—	—	0.543	0.224	34.531	0.582
	3 Brs	—	—	0.443	0.185	32.880	0.599
DWT	Healthy	0.229	0.014	—	—	16.357	0.074
	1 Br	0.265	−0.012	—	—	−22.083	0.074
	2 Brs	0.221	0.090	—	—	2.456	0.098
	3 Brs	0.270	0.003	—	—	90	0.100
SS	Healthy	—	—	0.036	0.064	0.100	0.626
	1 Br	—	—	0.423	0.056	3.255×10^3	0.583
	2 Brs	—	—	0.618	0.073	5.136×10^3	0.606
	3 Brs	—	—	0.598	0.064	7.622×10^3	0.608

averaged IM condition indicators and running time over 20 runs are summarized in Table II. The values of slip for IMs with healthy condition, one broken bar, two broken bars, and three broken bars are 0.025, 0.026, 0.026, and 0.025, respectively. It is seen that the relative amplitude of fault frequency component in Fig. 6(b)–(d) is greater than that in Fig. 6(a). From Table II, it is seen that DWT cannot effectively differentiate IM fault. On the other hand, the IM broken rotor bar fault condition cannot be differentiated from healthy condition using PSD, because the indicator values χ are similar for different IM health conditions. The fault indicator χ_s related to the proposed SS technique can accurately discern the healthy condition and broken rotor bar fault, and its χ_s value increases as the number of broken bars increases.

C. Incipient Bearing Defect Detection

The type of bearings used in the test IMs is NSK6203. As mentioned earlier, the bearing defects are the most common faults in IMs [2], which also represent the most challenging task in IM health condition monitoring, especially when using current signals [13]–[15]. Pitting defect is induced on the outer race of the bearing. Whenever a rolling element rolls over the damaged region, impulses are generated, which then excite the resonance frequencies of the IM structure.

The IM characteristic frequency depends on rolling element bearing geometry (e.g., number of rolling elements N_b, pitch diameter D, roller diameter d) and shaft speed f_r. The vibration-related outer race bearing defect characteristic frequency f_v can

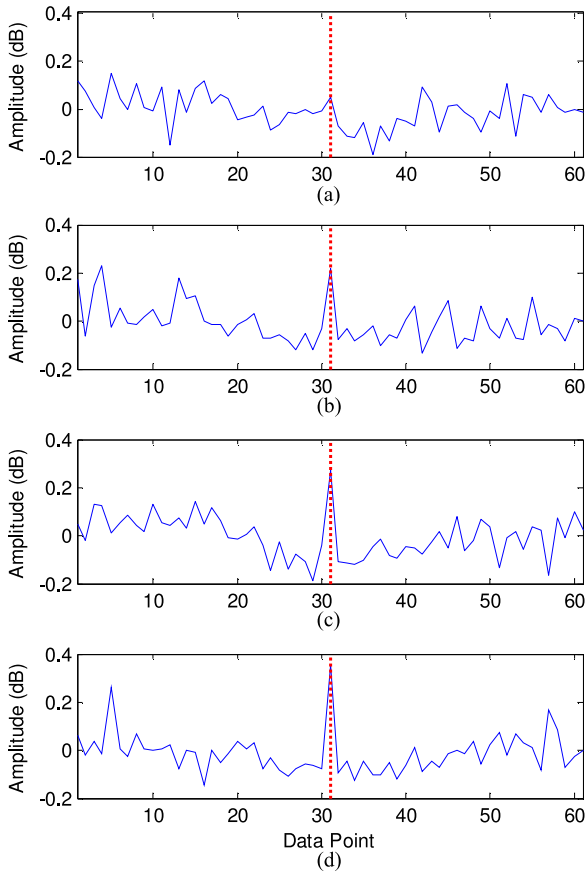

Fig. 6. FIS generated by the SS technique under half-load condition from: (a) healthy IM; (b) IM with one broken rotor bar; (c) IM with two broken rotor bars; and (d) IM with three broken rotor bars.

TABLE II
COMPARISONS OF MEAN VALUES OF INDICATORS FOR IM BROKEN ROTOR BAR FAULT DETECTION OVER 20 RUNS UNDER HALF-LOAD CONDITION

Indicators		$F_c(A)$	$E_c(A)$	v (dB)	σ (dB)	χ	Time (s)
PSD	Healthy	—	—	0.193	0.190	1.065	0.593
	1 Br	—	—	0.249	0.184	3.354	0.615
	2 Brs	—	—	0.308	0.186	7.519	0.607
	3 Brs	—	—	0.335	0.212	6.235	0.614
DWT	Healthy	0.197	−0.027	—	—	7.296	0.077
	1 Br	0.122	−0.056	—	—	−2.179	0.079
	2 Brs	0.190	0.007	—	—	27.143	0.086
	3 Brs	0.178	−0.042	—	—	−4.238	0.074
SS	Healthy	—	—	0.059	0.072	0.451	0.623
	1 Br	—	—	0.234	0.077	85.291	0.630
	2 Brs	—	—	0.282	0.080	154.396	0.590
	3 Brs	—	—	0.372	0.070	797.590	0.581

be computed by

$$f_v = \frac{N_b}{2}\left(1 - \frac{d\cos(\theta)}{D}\right) f_r \tag{14}$$

where θ is the contact angle.

The corresponding characteristic current frequency f_c can be calculated from

$$f_c = |f_p \pm m f_v| \tag{15}$$

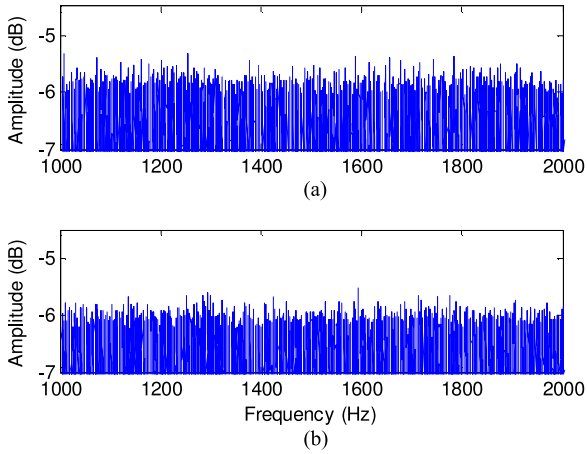

Fig. 7. Spectrum average Φ from (a) healthy IM and (b) IM with the outer race bearing defect, under no-load condition.

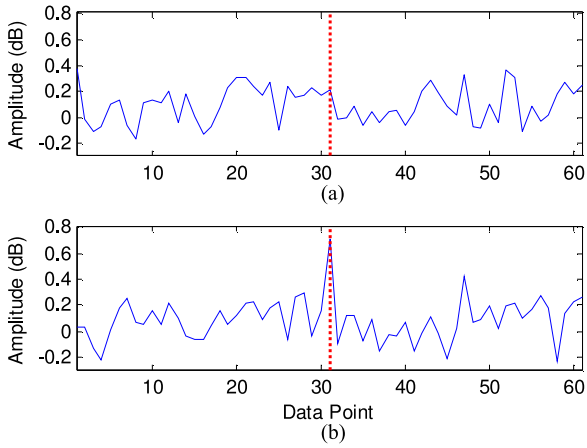

Fig. 8. FIS generated by the SS technique under no-load condition: (a) from a healthy IM; and (b) from an IM with the outer race bearing defect.

where f_p is the power supply frequency, and $m = 1, 2, 3, \ldots,$ is a positive integer.

1) No-Load Condition: The proposed SS technique is first tested with current signals collected from an IM with an outer race defect, 50 Hz power supply frequency, and no-load condition (0% of rated power). The settings for the proposed SS technique are selected as $J = 20$, $f_s = 16\,384$ Hz, $b_w = 6$ Hz, and $f_v = 3.066 f_r$. To obtain representative fault features, the frequency band [1000 Hz, 2000 Hz] is selected for bearing fault detection.

The frequency band [1000 Hz 2000 Hz] from a healthy IM and an IM with outer race bearing defect is shown in Fig. 7(a) and (b), respectively. It is seen that the bearing fault frequency components are difficult to recognize due to the modulation of the signals with other IM frequency components.

The FIS, corresponding to a healthy IM and an IM with the outer race defect, is given in Fig. 8(a) and (b), respectively. The values of indicators corresponding to three fault detection techniques PSD, DWT, and SS and running time are summarized in Table III. It is seen from Fig. 8 that the fault frequency

TABLE III
COMPARISONS OF MEAN VALUES OF INDICATORS FOR IM BEARING FAULT DETECTION OVER 20 RUNS UNDER NO-LOAD CONDITION

Indicators		$E_c(A)$	$F_c(A)$	v (dB)	σ (dB)	χ	Time (s)
PSD	Healthy	—	—	0.105	0.131	0.413	0.226
	Bearing fault	—	—	0.134	0.122	1.455	0.166
DWT	Healthy	0.013	−0.040	—	—	−0.325	0.072
	Bearing fault	0.011	0.098	—	—	0.112	0.071
SS	Healthy	—	—	0.117	0.141	0.474	0.181
	Bearing fault	—	—	0.527	0.140	200.785	0.146

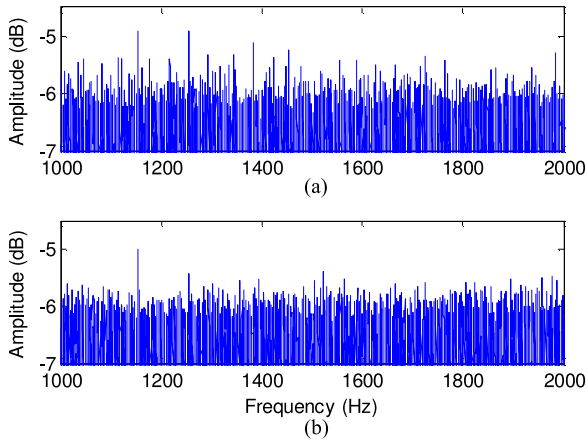

Fig. 9. Spectrum average Φ from (a) healthy IM and (b) IM with the outer race bearing defect, under light-load condition.

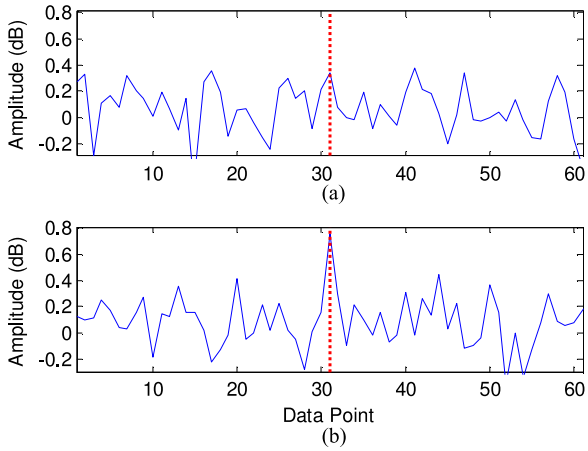

Fig. 10. FIS generated by the SS technique under light-load condition: (a) from a healthy IM; and (b) from an IM with the outer race bearing defect.

TABLE IV
COMPARISONS OF MEAN VALUES OF INDICATORS FOR IM BEARING FAULT DETECTION OVER 20 RUNS UNDER LIGHT-LOAD CONDITION

Indicators		$E_c(A)$	$F_c(A)$	v (dB)	σ (dB)	χ	Time (s)
PSD	Healthy	—	—	0.007	0.160	0	0.166
	Bearing fault	—	—	0.167	0.149	1.578	0.169
DWT	Healthy	0.012	0.098	—	—	0.122	0.075
	Bearing fault	0.014	−0.032	—	—	−0.438	0.081
SS	Healthy	—	—	0.270	0.188	4.254	0.142
	Bearing fault	—	—	0.570	0.175	112.550	0.147

component in Fig. 8(b) protrudes more significantly than that in Fig. 8(a). In Table III, the fault indicator χ_s of the IM with faulty bearing is greater than that of a healthy IM using the proposed SS technique, whereas the PSD and DWT cannot recognize different IM health conditions. Therefore, the SS technique can be used effectively for IM outer race bearing fault detection under no-load condition.

2) Light-Load Condition: In this test, the IM supply frequency is set as 50 Hz, and light-load condition (20% of rated power) is used. The other settings remain the same as in previous test. The frequency band [1000 Hz 2000 Hz] of an IM with the outer race bearing defect is used for testing. The band [1000 Hz 2000 Hz] is shown in Fig. 9, corresponding to a healthy IM [see Fig. 9(a)] and an IM with the bearing defect [see Fig. 9(b)]. From Fig. 9, the bearing fault frequency components in the spectrum are masked by higher amplitude frequency components unrelated to the bearings, which will reduce the fault detection reliability.

The FIS of a healthy IM and an IM with outer race bearing defect is shown in Fig. 10. The indicators of PSD, DWT, and the proposed SS technique and running time are listed in Table IV. It is seen that peaked center frequency component can be highlighted in Fig. 10(b) than in (a). From Table IV, it is seen that the values of χ_s in the proposed SS technique is much greater than that from a healthy IM. Thus, the SS technique and its indicator χ_s can be used for IM outer race bearing defect detection under different load conditions.

IV. CONCLUSION

An SS technique has been proposed in this paper for IM fault detection using stator current signals. This research focuses on broken rotor bar fault and outer race bearing fault detection. The local band synch technique is employed to synthesize bearing fault-related features to form an FIS to enhance IM defect-related features. A central kurtosis analysis method is proposed to extract features from the FIS, which are then used to formulate a fault indicator. The effectiveness of the proposed IM fault detection technique is verified using IMs with the bearing defect and different broken rotor bars, under different load conditions. Test results showed that the proposed SS technique and the related central kurtosis indicator can capture IM defect features effectively and can provide more accurate IM health condition monitoring information. Further research is underway to verify and improve the effectiveness of the proposed technique using larger horsepower IMs.

REFERENCES

[1] M. E. H. Benvouzid, "A review of induction motors signature analysis as a medium for faults detection," *IEEE Trans. Ind. Electron.*, vol. 47, no. 5, pp. 984–993, Oct. 2000.
[2] P. J. Tavner, "Review of condition monitoring of rotating electrical machines," *IET Elect. Power Appl.*, vol. 2, no. 4, pp. 215–247, 2008.
[3] Y. H. Kim, Y. W. Youn, D. H. Hwang, J. H. Sun, and D. S. Kang, "High-resolution parameter estimation method to identify broken rotor bar faults in induction motors," *IEEE Trans. Ind. Electron.*, vol. 60, no. 9, pp. 4103–4117, Sep. 2013.

[4] B. Akin, U. Orguner, H. A. Toliyat, and M. Rayner, "Phase-sensitive detection of motor fault signatures in the presence of noise," *IEEE Trans. Ind. Electron.*, vol. 55, no. 6, pp. 2539–2550, Jun. 2008.
[5] O. Poncelas, J. A. Rosero, J. Cusido, J. A. Ortega, and L. Romeral, "Motor fault detection using a Rogowski sensor without an integrator," *IEEE Trans. Ind. Electron.*, vol. 56, no. 10, pp. 4062–4070, Oct. 2009.
[6] A. Bellini, F. Immovilli, R. Rubini, and C Tassoni, "Diagnosis of bearing faults of induction machines by vibration or current signals: A critical comparison," in *Proc. IEEE Ind. Appl. Soc. Annu. Meeting*, 2008, pp. 1–8.
[7] N. Tando, G. S. Yadava, and K. M. Ramakrishna, "A comparison of some condition monitoring techniques for the detection of defect in induction motor ball bearings," *Mech. Syst. Signal Process.*, vol. 21, no. 1, pp. 244–256, 2007.
[8] A. M. Knight and S. P. Bertani, "Mechanical fault detection in a medium-sized induction motor using stator current monitoring," *IEEE Trans. Energy Convers.*, vol. 20, no. 4, pp. 753–760, Dec. 2005.
[9] E. C. C. Lau and H. W. Ngan, "Detection of motor bearing outer raceway defect by wavelet packet transformed motor current signature analysis," *IEEE Trans. Instrum. Meas.*, vol. 59, no. 10, pp. 2683–2690, Oct. 2010.
[10] A. Lebaroud and G. Clerc, "Classification of induction machine faults by optimal time-frequency representations," *IEEE Trans. Ind. Electron.*, vol. 55, no. 12, pp. 4290–4298, Dec. 2008.
[11] R. R. Schoen, T. G. Habetler, F. Kamran, and R. Bartheld, "Motor bearing damage detection using stator current monitoring," *IEEE Trans. Ind. Appl.*, vol. 31, no. 6, pp. 1274–1279, Nov./Dec. 1995.
[12] M. Blödt, P. Granjon, B. Raison, and G. Rostaing, "Models for bearing damage detection in induction motors using stator current monitoring," *IEEE Trans. Ind. Electron.*, vol. 55, no. 4, pp. 1813–1822, Apr. 2008.
[13] J. Ilonen, J. K. Kamarainen, T. Lindh, J. Ahola, H. Kalviainen, and J. Partanen, "Diagnosis tool for motor condition monitoring," *IEEE Trans. Ind. Appl.*, vol. 41, no. 4, pp. 963–971, Jul./Aug. 2005.
[14] L. Eren and M. J. Devaney, "Bearing damage detection via wavelet packet decomposition of the stator current," *IEEE Trans. Instrum. Meas.*, vol. 53, no. 2, pp. 431–436, Apr. 2004.
[15] W. Zhou, B. Lu, T. G. Habetler, and R. G. Harley, "Incipient bearing fault detection via motor stator current noise cancellation using Wiener filter," *IEEE Trans. Ind. Appl.*, vol. 45, no. 4, pp. 1309–1317, Jul./Aug. 2009.
[16] B. Kim, K. Lee, J. Yang, S. B. Lee, E. J. Wiedenbrug, and M. R. Shah, "Automated detection of rotor faults for inverter-fed induction machines under standstill conditions," *IEEE Trans. Ind. Appl.*, vol. 47, no. 1, pp. 55–64, Jan./Feb. 2011.
[17] A. Ordaz-Moreno, R. J. Romero-Troncoso, J. A. Vite-Frias, J. R. Rivera-Gillen, and A. Garcia-Perez, "Automatic online diagnosis algorithm for broken-bar detection on induction motors based on discrete wavelet transform for FPGA implementation," *IEEE Trans. Ind. Electron.*, vol. 55, no. 5, pp. 2193–2202, May 2008.
[18] B. Ayhan, H. J. Trussell, M. Y. Chow, and M. H. Song, "On the use of a lower sampling rate for broken rotor bar detection with DTFT and AR-based spectrum methods," *IEEE Trans. Ind. Electron.*, vol. 55, no. 3, pp. 1421–1434, Mar. 2008.
[19] M. Haji and A. Toliyat, "Pattern recognition—A technique for induction machines rotor broken bar detection," *IEEE Trans. Energy Convers.*, vol. 16, no. 4, pp. 312–317, Dec. 2001.
[20] Z. Zhang, Z. Ren, and W. Huang, "A novel detection method of motor broken rotor bars based on wavelet ridge," *IEEE Trans. Energy Convers.*, vol. 18, no. 3, pp. 417–423, Sep. 2003.
[21] Y. Kim, Y. Youn, D. Hwang, J. Sun, and D. Kang, "High-resolution parameter estimation method to identify broken rotor bar faults in induction motors," *IEEE Trans. Ind. Electron.*, vol. 60, no. 9, pp. 4103–4117, Sep. 2013.
[22] A. Soualhi, G. Clerc, and H. Razik, "Detection and diagnosis of faults in induction motor using an improved artificial ant clustering technique," *IEEE Trans. Ind. Electron.*, vol. 60, no. 9, pp. 4053–4062, Sep. 2013.
[23] J. D. J. Rangel-Magdaleno, H. Peregrina-Barreto, J. M. Ramirez-Cortes, P. Gomez-Gil, and R. Morales-Caporal, "FPGA-based broken bars detection on induction motors under different load using motor current signature analysis and mathematical morphology," *IEEE Trans. Instrum. Meas.*, vol. 63, no. 5, pp. 1032–1040, May 2014.
[24] B. Xu, L. Sun, L. Xu, and G. Xu, "Improvement of the Hilbert method via ESPRIT for detecting rotor fault in induction motors at low slip," *IEEE Trans. Energy Convers.*, vol. 28, no. 1, pp. 225–233, Mar. 2013.
[25] W. H. Press, S. Teukolsky, W. T. Vetterling, and B. P. Flannery, *Numerical Recipes 3rd Edition: The Art of Scientific Computing*. Cambridge, U.K.: Cambridge Univ. Press, 2007.
[26] B. M. Ebrahimi, J. Faiz, S. Lotfi-fard, and P. Pillay, "Novel indices for broken rotor bars fault diagnosis in induction motors using wavelet transform," *Mech. Syst. Signal Process.*, vol. 30, pp. 131–145, 2012.

De Z. Li received the B.Sc. degree in electrical engineering from Shandong University, Jinan, China, in 2008, and the M.Sc. degree in control engineering from Lakehead University, Thunder Bay, ON, Canada, in 2010. He is currently working toward the Ph.D. degree in the Department of Mechanical and Mechatronics Engineering, University of Waterloo, Waterloo, ON.

From 2010 to 2011, he was a Research Associate at Lakehead University. His research interests include machinery health condition monitoring, signal processing, machine learning, mechatronic systems, linear/nonlinear system control, and artificial intelligence.

Wilson Wang (M'04–SM'07) received the M.Eng. degree in industrial engineering from the University of Toronto, Toronto, ON, Canada, in 1998, and the Ph.D. degree in mechatronics engineering from the University of Waterloo, Waterloo, ON, in 2002.

From 2002 to 2004, he was a Senior Scientist with Mechworks Systems, Inc., Waterloo. He joined the faculty of Lakehead University, Thunder Bay, ON, in 2004, where he is currently a Professor in the Department of Mechanical Engineering. His research interests include signal processing, artificial intelligence, machinery condition monitoring, intelligent control, and mechatronics.

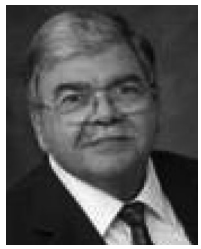

Fathy Ismail received the B.Sc. and M.Sc. degrees in mechanical and production engineering from Alexandria University, Alexandria, Egypt, in 1970 and 1974, respectively, and the Ph.D. degree in mechanical engineering from McMaster University, Hamilton, ON, Canada, in 1983.

He joined the University of Waterloo, Waterloo, ON, in 1983, and is currently a Professor in the Department of Mechanical and Mechatronics Engineering. He has served as the Chair of the department and the Associate Dean of the Faculty of Engineering for Graduate Studies. His research interests include machining dynamics, high-speed machining, modeling structures from modal analysis testing, and machinery health condition monitoring and diagnosis.